Efficient method to simulate non-perturbative dynamics of an open quantum system using a quantum computer

José D. Guimarães*

Centro de Física das Universidades do Minho e do Porto, Laboratório de Física para Materiais e Tecnologias Emergentes (LaPMET), Universidade do Minho, Braga 4710-057, Portugal and International Iberian Nanotechnology Laboratory, Av. Mestre José Veiga s/n, Braga 4715-330, Portugal

Mikhail I. Vasilevskiy

Centro de Física das Universidades do Minho e do Porto, Laboratório de Física para Materiais e Tecnologias Emergentes (LaPMET) and Departamento de Física, Universidade do Minho, Braga 4710-057, Portugal and International Iberian Nanotechnology Laboratory, Av. Mestre José Veiga s/n, Braga 4715-330, Portugal

Luís S. Barbosa

INESC TEC, Departamento de Informática, Universidade do Minho, Braga 4710-057, Portugal and International Iberian Nanotechnology Laboratory, Av. Mestre José Veiga s/n, Braga 4715-330, Portugal

Classical non-perturbative simulations of open quantum systems dynamics face several scalability problems, namely, exponential scaling as a function of either the time length of the simulation or the size of the open system. In this work, we propose a quantum computational method which we term as Quantum Time Evolving Density operator with Orthogonal Polynomials Algorithm (Q-TEDOPA), based on the known TEDOPA technique, avoiding any exponential scaling in simulations of non-perturbative dynamics of open quantum systems on a quantum computer. By performing an exact transformation of the Hamiltonian, we obtain only local nearest-neighbour interactions, making this algorithm suitable to be implemented in the current Noisy-Intermediate Scale Quantum (NISQ) devices. We show how to implement the Q-TEDOPA using an IBM quantum processor by simulating the exciton transport between two light-harvesting molecules in the regime of moderate coupling strength to a non-Markovian harmonic oscillator environment. Applications of the Q-TEDOPA span problems which can not be solved by perturbation techniques belonging to different areas, such as dynamics of quantum biological systems and strongly correlated condensed matter systems.

I. INTRODUCTION

The emergence of decoherence in quantum systems is an important and ubiquitous phenomenon in Nature because any real system is never completely isolated. On the other hand, Hamiltonian dynamics simulation of such a system is by no means trivial, since its environment typically involves an intractable number of degrees of freedom. Approximations are thus usually employed, however they limit the range of applications of the computational method. Hence, non-perturbative methods have been proposed to be applied to general open quantum systems, in particular the ones where perturbative techniques fail. One of such techniques is the Hierarchical Equations of Motion (HEOM) [1], which is rather successful at simulating open quantum systems dynamics at room-temperature [2, 3]. However, it exhibits exponential scaling with the size of the system [1]. On the other hand, the Time Evolving Density operator with Orthogonal Polynomials Algorithm (TEDOPA) [4–6], or its more recent extension Thermalized TEDOPA (T-TEDOPA) [7], avoids such an intractable scaling by making use of Matrix Product States (MPS) at simulating dynamics of one-dimensional quantum systems [7]. The main bottleneck of this technique lies in the scaling of the bond dimension of the MPS, which typically increases exponentially as a function of time [8, 9], hence long-time simulations are hard to reach via this technique. Simulations of higher-dimensional systems are also difficult to be implemented using MPS, incurring in an exponential scaling as a function of the size of the system [8]. The crucial point is that classical simulations of open quantum systems dynamics are limited by unfavorable scalings relatively to the system's size or time length of the simulation.

One possible alternative approach is to use quantum computing to simulate open quantum systems. Current Noisy-Intermediate Scale Quantum (NISQ) computers are hampered by noisy hardware, low qubit count and time-expensive access. Hence, quantum digital simulations have only been able to be applied to small quantum systems [10, 11]. Nevertheless, as quantum hardware and

^{*} Email for correspondence: josediogo176@gmail.com

software improves, speedups relatively to classical simulation are expected to be observed (and some problems solved by quantum computing have been already shown to beat classical computing by a large factor [12, 13]). In the context of quantum digital simulations of open quantum systems, several techniques have recently been proposed, such as using Kraus operators [14–18], solving the Lindblad equation with stochastic Schrödinger equations [19] or variationally [20], using the inherent decoherence of the quantum computer to implement the dissipative evolution [21, 22], among others [23–26]. These techniques face some important issues, namely, the Kraus operators are hard to calculate in practice, Lindblad equations are restricted to Markovian environments and the natural decoherence of the quantum computer introduced by the qubits' environment is not fully controllable or its structure is not completely known, hence simulating arbitrary environments is hard.

In this work, we propose a new quantum method to simulate non-perturbative dynamics of open quantum systems, the Quantum Time Evolving Density operator with Orthogonal Polynomials Algorithm (Q-TEDOPA). This technique is based on an exact transformation of the environment and system-environment interaction Hamiltonians. The open quantum system simulation is mapped to a problem of closed Hamiltonian dynamics which can be efficiently simulated in a quantum computer. This method avoids the difficulties mentioned above, which other quantum algorithms face, drastically improves the efficiency of open quantum systems' simulation over the classical TEDOPA, and can be efficiently implemented in the NISQ computers. In Section II, we briefly review the TEDOPA technique. In Section III, we describe how to implement the TEDOPA on a quantum computer (Q-TEDOPA) and analyze its complexity. Lastly, in Section IV, we apply the Q-TEDOPA to the exciton transport between two light-harvesting molecules in a quantum processor based on superconductor gubits, provided by IBM.

II. REVISITING THE TEDOPA

Consider an open quantum system composed by some entities (such as molecules) interacting between themselves and with an environment. The total Hamiltonian of such a system can be written as

$$H = H_S + H_E + H_{SE} \,, \tag{1}$$

where H_S , H_E and H_{SE} are the open quantum system, the environment, and the system-environment interaction Hamiltonians, respectively.

We define the environment as a continuum of harmonic oscillators at temperature T=0K and the system-

environment interaction Hamiltonian reads as follows [7],

$$H_E = \int_0^\infty d\omega \omega a_\omega^{\dagger} a_\omega, \tag{2}$$

$$H_{SE} = \hat{A} \otimes \int_0^\infty d\omega \sqrt{J(\omega)} (a_\omega^\dagger + a_\omega).$$
 (3)

The operator \hat{A} , which form will be defined later, acts only upon the open quantum system's Hilbert subspace. The operator a_{ω}^{\dagger} (a_{ω}) is the phonon creation (annihilation) operator associated to a mode with frequency ω , such that $[a_{\omega}, a_{\omega'}^{\dagger}] = \delta(\omega - \omega')$ and $[a_{\omega}, a_{\omega}] = [a_{\omega}^{\dagger}, a_{\omega}^{\dagger}] = 0$. The spectral density $J(\omega)$ defines the system-environment coupling (squared) times the density of states of the bath [4].

We now apply an exact transformation to the environment operators as follows [4, 5, 7],

$$b_n^{\dagger} = \int_0^{\infty} d\omega U_n(\omega) a_{\omega}^{\dagger}, \quad n = 0, 1, \dots$$
 (4)

and the same operation to the phonon annihilation operator a_{ω} , yielding b_n . The resulting operators b_n^{\dagger} and b_n preserve the bosonic commutation relations, i.e. $[b_n, b_m^{\dagger}] = \delta_{nm}$ and $[b_n, b_m] = [b_n^{\dagger}, b_m^{\dagger}] = 0$. The transformation $U_n(\omega)$ is given in references [4, 5] by

$$U_n(\omega) = \sqrt{J(\omega)} p_n(\omega) , \qquad (5)$$

where $p_n(\omega)$ is an orthogonal polynomial with respect to the measure $d\mu = J(\omega)d\omega$ defined in the domain $\omega \in [0,\infty[$, i.e. $\int_0^\infty p_n(\omega)p_m(\omega)d\mu(\omega) = \delta_{nm}$.

Using the orthogonal polynomial recurrence relation [5] and the definition of an orthogonal polynomial presented above, one can exactly map the environment and interaction Hamiltonians [5] to:

$$H_{SE}^{C} = t_0 \hat{A} \otimes (b_0^{\dagger} + b_0),$$
 (6)

$$H_E^C = \sum_{n=0}^{\infty} w_n b_n^{\dagger} b_n + \sum_{n=1}^{\infty} t_{n,n-1} b_n^{\dagger} b_{n-1} + h.c., \qquad (7)$$

where the Hamiltonian coefficients t_0 , w_n and $t_{n,n-1}$ can be obtained from the orthogonal polynomial recurrence coefficients. The TEDOPA Hamiltonian transformation is illustrated in Fig. 1 for a two- and three-site coupled open quantum system. We define $H^C = H_{SE}^C + H_E^C$ as the chain Hamiltonian.

In order to map the Hamiltonians given in equations (2) and (3) to the chain Hamiltonian, the recurrence coefficients of the orthogonal polynomials defined with respect to the measure $d\mu(\omega) = J(\omega)d\omega$ must be calculated. They can be obtained analytically for strict Ohmic baths [5], or, in general, through a numerically efficient algorithm, available in the ORTHPOL package [27].

Some remarks about the exact TEDOPA transformation are in order: (i) commutation and anti-commutation relations of the initial bath operators are preserved after

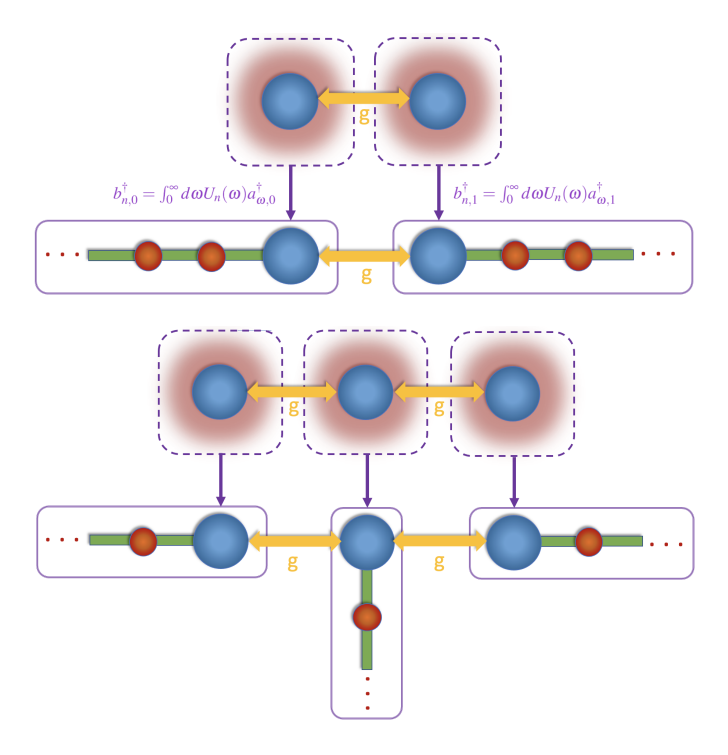


FIG. 1: (a) TEDOPA Hamiltonian transformation. Initially, the two sites (blue circles) are coupled with interaction strength g and each site interacts with its own identical harmonic oscillator environment (red blur surrounding the sites). The TEDOPA transformation is applied to each environment and site-environment interaction Hamiltonians, i.e. to the environmental operators a_{ω}^{\dagger} and a_{ω} , such that the resultant model comprises a nearest-neighbour semi-infinite one-dimensional system representing the environment. On the left (right) edge of the one-dimensional system, one has a chain of harmonic oscillators coupled to the first (second) site. This chain represents the environment, where each red circle is a harmonic oscillator. (b) Same as (a), but now having three coupled sites. A one-dimensional system is not obtained after applying the TEDOPA Hamiltonian transformation, hence MPS-based simulations are no longer efficient.

the transformation. This means that one can also simulate, for instance, fermionic baths. (ii) If we define a spectral density belonging to the Szegö class [28] with hard frequency cutoffs ω_{min} and ω_{max} , the chain Hamiltonian coefficients converge [28, 29] to,

$$\lim_{n \to \infty} w_n = \frac{\omega_{max} + \omega_{min}}{2}, \tag{8}$$

and,

$$\lim_{n \to \infty} t_{n,n-1} = \frac{\omega_{max} - \omega_{min}}{4}.$$
 (9)

(iii) The generalization of TEDOPA to nonzero temperature environments has been termed Thermalized

TEDOPA (T-TEDOPA) [7]. It consists in defining a temperature-dependent spectral density [7] as follows,

$$J_{\beta}(\omega) = sign(\omega) \frac{J(|\omega|)}{2} \left(1 + \coth\left(\frac{\beta\omega}{2}\right) \right) . \tag{10}$$

The T-TEDOPA transformation, in contrast with equation (4), is given by:

$$b_{\beta,n}^{\dagger} = \int_{-\infty}^{\infty} d\omega U_{\beta,n}(\omega) a_{\omega}^{\dagger}, \quad n = 0, 1, \dots,$$
 (11)

where $\beta^{-1} = k_B T$ and $U_{\beta,n}(\omega) = \sqrt{J_{\beta}(\omega)} p_{\beta,n}(\omega)$, such that the temperature-dependent orthogonal polynomials are defined with respect to the measure $d\mu_{\beta}(\omega) = J_{\beta}(\omega)d\omega$. The initial state of the harmonic oscillators in the chain is always set to the vacuum state, following reference [7].

III. QUANTUM TEDOPA

A. Implementation

The basic insight is that the evolution operator of the total Hamiltonian $H = H_S + H^C$ can be efficiently implemented in a quantum computer. In order to do that, the chain must be truncated to some number, l, of harmonic oscillators in it, and each harmonic oscillator must be truncated to a d-dimensional site (allowing up to (d-1)phonons for a site n). The number of phonon states, d, depends on the structure of the spectral density, i.e. it is specific for a given problem, as investigated in reference [29]. One possible approach to find the minimum land d that allow us to simulate numerical exact results, is to simulate the system for a time t with an initial guess of l d-dimensional harmonic oscillators, measure the desired observable \hat{O} , and then repeat the simulation procedure for a time t, with l' > l of d'-dimensional harmonic oscillators with d' > d. Choosing a small error threshold $\epsilon > 0$, numerical exact results are obtained if $|\langle \hat{O} \rangle_t - \langle \hat{O}' \rangle_t| < \epsilon$, where \hat{O}' is the measured observable in the simulation with the increased chain dimensions d'and l'.

To simulate the Hamiltonian dynamics, the environment creation and annihilation operators obtained in equation (4) must be mapped to Pauli operators so that the chain of harmonic oscillators is appropriately encoded in a quantum circuit. As extensively studied in reference [30], choosing a particular bosonic qubit encoding may change how the number of necessary quantum gates and qubits to simulate the system scale in the asymptotic limit of l and d tending to infinity. In Appendix A, we describe how to map bosonic operators to Pauli operators using the unary and binary qubit encodings and the scaling of these transformations as a function of the size of the harmonic oscillator chain.

Having the chain Hamiltonian written in terms of Pauli operators as discussed in Appendix A, one can perform

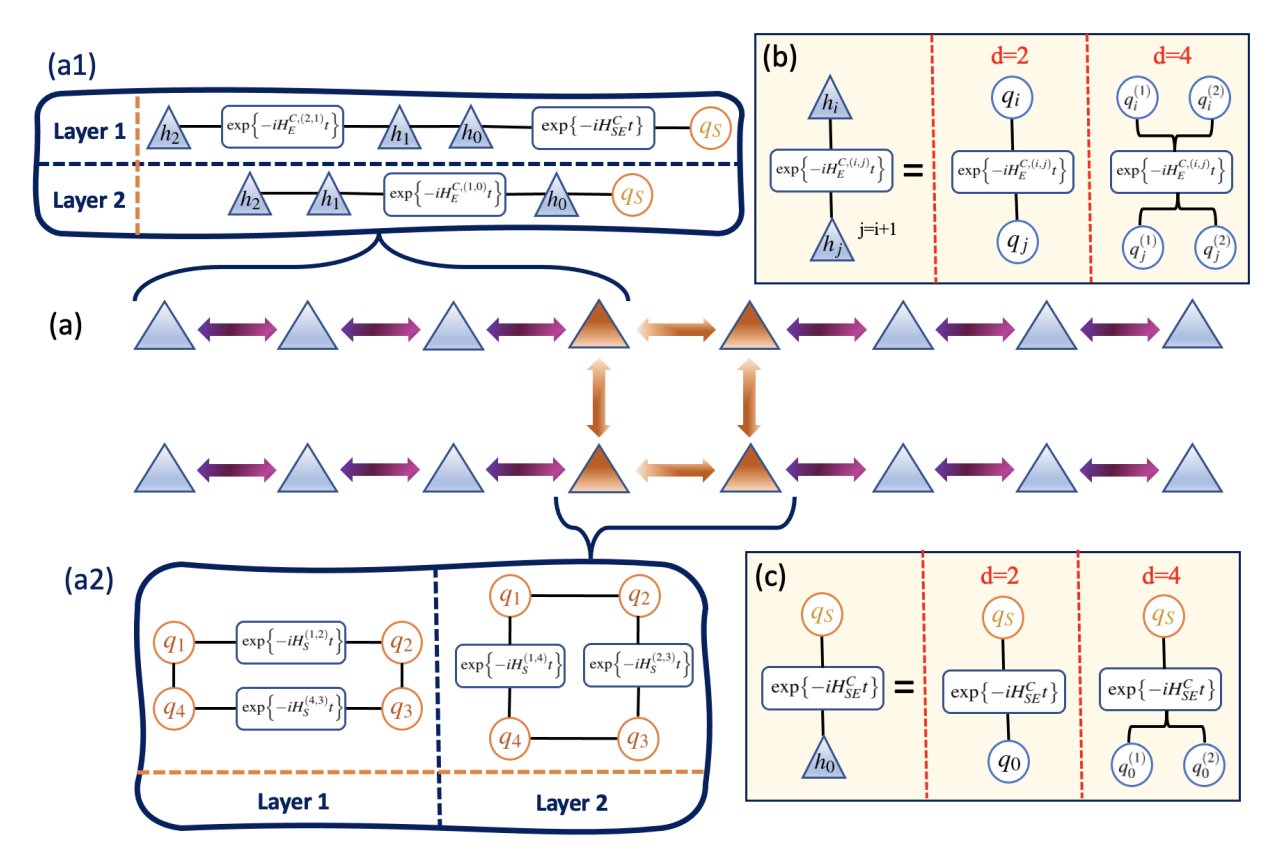


FIG. 2: Implementation of Q-TEDOPA. After applying the TEDOPA Hamiltonian transformation, one obtains a nearest-neighbour interaction model as shown in (a). (a) Open quantum system composed of 4 two-level molecules (orange triangles) with nearest-neighbour interactions as illustrated by the orange arrows. Each molecule interacts with a chain of harmonic oscillators truncated to three here (represented by blue triangles). Purple arrows represent the two-site interactions in the chain Hamiltonian H^C . Inside the boxes (a1) and (a2), we show the types of two-qubit gate layers that are encoded in the quantum circuit to simulate the evolution of the total system via the Trotter-Suzuki product formula. These are illustrated for the chain Hamiltonian in the box (a1) and for the open quantum system Hamiltonian in the box (a2). Orange circles represent the molecules of the open quantum system encoded as qubits. (b) Example of the implementation of the interaction between harmonic oscillators h_i and h_j , with j = i + 1, mapped to sets of qubits q_i and q_j , respectively. We illustrate the implementation of this interaction in a quantum circuit for d = 2 and d = 4 binary qubit encodings of the harmonic oscillators (more details in Appendix A). (c) Same as (b) but for the molecule-harmonic oscillator interaction.

the time evolution with an efficient quantum algorithm that performs closed Hamiltonian dynamics simulations. This is an additional advantage of Quantum TEDOPA over existent proposals of quantum methods to simulate open quantum systems, because the problem of simulating the open quantum system is transformed into a problem of simulating a closed one. This is specially relevant for quantum computing, since the quantum gates available to perform the computation are unitary. To simulate the system in a quantum computer, the evolution operator may be decomposed with Trotter-Suzuki decompositions [31, 32], truncated Taylor series [33] or qubitization and quantum signal processing techniques [34]. The simulations performed with these decomposition techniques typically require long coherence times in the current NISQ computers in order to produce faithful results. Therefore, one may instead simulate the closed Hamiltonian dynamics via hybrid quantum-classical methods, such as the Variational Quantum Simulator [20, 35], Variational Fast-Forwarding methods [36, 37] or variational compressed Trotter techniques [38, 39].

We remark that the chain Hamiltonian is local, in the sense that it exhibits only nearest-neighbour interactions in the environment Hilbert subspace. On quantum hardware, a d-dimensional harmonic oscillator is encoded in a set of qubits. For d=2, only one qubit per harmonic oscillator is required. This means that the resulting quantum circuit to simulate the dynamics exhibits solely nearest-neighbour qubit-qubit interactions as shown in Figure 2. For d-dimensional harmonic oscillators, where d>2, the range of qubit-qubit interactions is, in the worst case, 2d-local for unary encoding and $2\log(d)$ -local for binary encoding. Typically, no very large dimensions d are required (even for room-temperature calcu-

lations using T-TEDOPA) [7, 29]. Hence, Q-TEDOPA can be efficiently implemented on quantum hardware with restricted qubit connectivity such as superconducting quantum processors. In Figure 2, we illustrate how Q-TEDOPA can be implemented for a four-site open quantum system, where each site is coupled to a harmonic oscillator environment.

B. Comparison of the complexity of the Q-TEDOPA and TEDOPA

Simulations of Hamiltonian dynamics with the TEDOPA in a classical computer are usually performed using techniques based in Matrix Product States (MPS) for one-dimensional systems, such as the Time-Evolving Block Decimation (TEBD) algorithm [7, 8]. Up to our knowledge, the best complexity of the TEBD achieved at executing the TEDOPA has been reported to be $O(lN(dD)^3)$ [7]. We denote by N the number of Trotter iterations and by D the bond dimension of the MPS. The absence of an area law for entanglement entropy as a function of time for non-equilibrium systems' simulations [9] opens up the possibility of having the bond dimension exponentially scaling with time, i.e. $D \sim 2^t$, hence limiting classical simulations to short time lengths. Furthermore, in higher-dimensional systems, the problem persists and the bond dimension additionally incurs in a potential exponential scaling with the size of the system [8]. For instance, a simulation of the exciton transport across a chain of three light-harvesting molecules would be mapped into a two-dimensional system after applying the TEDOPA Hamiltonian transformation, as shown in Figure 1b. Therefore, this system is not efficiently simulated with MPS as the bond dimension would blow up exponentially with the size of the harmonic oscillator chain [8].

Q-TEDOPA does not face any of these issues. Choosing a first-order Trotter-Suzuki decomposition of the evolution operator as the time evolution method, one may simulate the dynamics with the number of quantum gates asymptotically scaling as $O(lNd^2)$ for unary qubit encoding and $O(lNd^2\log(d))$ for binary qubit encoding (see Appendix A). The number of qubits required to encode the chain in the simulation scales as O(ld) for unary qubit encoding and $O(l \log(d))$ for binary qubit encoding. Given the available noisy quantum hardware, one can trade a low qubit count for a higher circuit depth by adopting binary qubit encoding or the opposite with the choice of unary qubit encoding. One major advantage of Q-TEDOPA over classical TEDOPA is that the asymptotic scaling of quantum gates and qubits does not scale exponentially with time or size of the system, and this efficient behaviour is kept for simulations of higher-dimensional systems. A Q-TEDOPA simulation of a two-dimensional system performed with a Trotter-Suzuki product formula is exemplified in Figure 2. This shows that simulations of open quantum systems implemented on a quantum computer require exponentially less computational resources than with classical simulation, thus paving the way for efficient simulations of nonperturbative, general open quantum systems dynamics.

IV. NUMERICAL IMPLEMENTATION

We simulated the exciton transport between two electromagnetically coupled molecules of the photosynthetic Fenna-Matthews-Olsen (FMO) complex in green sulphur bacteria [40] in a proof-of-concept scenario. The Hamiltonian of the whole system is given by equation (1). The open quantum system Hamiltonian is composed of just two molecules and reads,

$$H_S = \sum_{m=0}^{1} \epsilon_m c_m^{\dagger} c_m + g \sum_{n \neq m} c_m^{\dagger} c_n, \qquad (12)$$

where ϵ_m is the energy of the excited state of molecule m, g is the electromagnetic coupling between the molecules, and c_m^{\dagger} (c_m) is the exciton creation (annihilation) operator applied to the molecule m. Appendix B reports the values of the Hamiltonian coefficients. We map the exciton operators to Pauli operators using a hardcore boson qubit encoding as explained in Appendix C.

We choose the \hat{A} operator in the interaction Hamiltonian (3) to be the Pauli operator \hat{Z} [41, 42], such that each molecule is coupled to an equivalent structured bath as follows $H_{SE} = \sum_{m} \hat{Z}_{m} \otimes \int_{0}^{\infty} d\omega \sqrt{J(\omega)} (a_{\omega,m}^{\dagger} + a_{\omega,m})$. The environment Hamiltonian is the one in equation (2). The bath is characterized by an exponentially decaying Ohmic spectral density at T = 0K of the form [5],

$$J(\omega) = 2\pi\alpha\omega e^{-\omega/\omega_c}\theta(\omega), \tag{13}$$

where $\alpha=0.25$ is an adimensional exciton-phonon coupling, $\omega_c=100~cm^{-1}$ is a soft cutoff frequency and $\theta(\omega)$ is the Heaviside step function. The hard cutoff frequency is chosen as $\omega_{max}=10\omega_c$ in order to have a negligible influence on the dynamics of the open quantum system (see Appendix B for more details). We remark that the chosen spectral density characterizes a non-Markovian environment, i.e. $J(\pm 2g) \not\approx const$ [41] and it exhibits a moderate open system-environment coupling, i.e. $J(\omega=g) \sim g$ [43] (the open quantum system's evolution timescale is set by g^{-1}). The environment and interaction Hamiltonians defined above are transformed to harmonic oscillator chains following the TEDOPA Hamiltonian transformation as described in Section II.

Figure 1a illustrates the simulated exciton transport model, where each site in the open quantum system is represented by a qubit, such that $|0\rangle$ and $|1\rangle$ represent the ground and excited states of a molecule, respectively. The phonon operators are mapped to Pauli operators following a d=2 (two energy levels) binary qubit encoding, hence each harmonic oscillator is represented by a qubit. A total of 5 harmonic oscillators in each chain

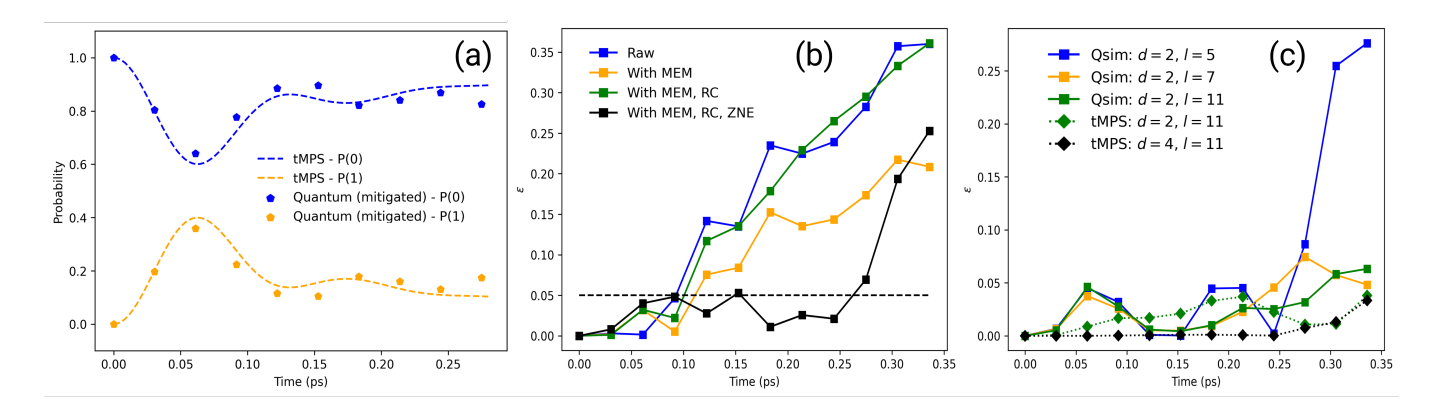


FIG. 3: (a) Mitigated results of the quantum digital simulation performed in the ibmq toronto (pentagons) and numerical exact results obtained with tMPS (dashed lines). P(0) (P(1)) denotes the probability of the exciton to be in the molecule 0 (1). (b) Error of the quantum simulation executed in the ibmq toronto when performed with and without quantum error mitigation techniques: Raw, MEM, RC and ZNE correspond to results obtained without error mitigation, with measurement error mitigation, with randomized compiling and with zero-noise extrapolation, respectively. The black dashed line corresponds to the upper bound of the error of the quantum simulation results (up to the 9th iteration). (c) Error of the classical simulations of quantum circuits without noise (Qsim) for different chain lengths. We also show the error of the results of the tMPS simulations (dotted lines) with chains of 11 two-dimensional and four-dimensional encoded harmonic oscillators (the remaining parameters of the simulation are reported in Appendix D).

were simulated. The initial state of the system is the environment at the vacuum state ($|0\rangle$ for all harmonic oscillator gubits) and the molecular gubits are initialized at state $|10\rangle$, i.e. the molecule 0 in the excited state and the molecule 1 in the ground state. The evolution of the open quantum system and the double chain of harmonic oscillators is performed using a first order Trotter-Suzuki product formula. The quantum digital simulation comprises a total of 12 qubits and about 400 implemented CNOT gates for 10 Trotter iterations. In order to obtain reliable results using the quantum hardware, several quantum error mitigation techniques have been implemented, namely, Qiskit measurement error mitigation [44], Randomized Compiling [45, 46] and Zero-Noise (exponential) Extrapolation [47, 48] via the Mitig package [49]. We used *Qiskit Runtime* to run the quantum simulation and the ibmq toronto quantum computer provided by IBM as our testbed. Lastly, we measured the probability of obtaining the states $|10\rangle$ and $|01\rangle$ in the molecular qubits, making use of the symmetry verification mitigation technique [50]. For more details on the implementation of the quantum simulation, we refer the reader to Appendix C.

The simulation results for 10 (12) Trotter iterations are shown in Figure 3 (in the Appendix C). We compared the quantum simulation results with the results obtained from a numerical exact tMPS simulation [8] (see Appendix D for more details). The quantum simulation results agree well with the classically computed numerical exact ones up to the 9th Trotter iteration, showing that the current quantum computers can already simulate non-perturbative dynamics of open quantum systems for

short time lengths. In Figure 3b, we plot the error of the quantum simulation when performed with and without the quantum error mitigation techniques. We define the simulation error as $\epsilon = |\langle \hat{O} \rangle_t^{(circ)} - \langle \hat{O} \rangle_t^{(num.exact)}| \in [0, 1]$ for $\langle \hat{O} \rangle_t = \langle \Psi(0)| e^{iHt} |01\rangle \langle 01| e^{-iHt} |\Psi(0)\rangle$, where $|\Psi(0)\rangle$ is the initial state of all the qubits in the system, and $\langle \hat{O} \rangle_t^{(circ)}$ and $\langle \hat{O} \rangle_t^{(num.exact)}$ are the measured expectation values in the quantum circuit and numerical exact tMPS simulations, respectively. We observed that the error of the results of the quantum mitigated simulation shown in Figure 3a is $\epsilon \lesssim 0.05$ up to the 9th Trotter iteration. If ZNE is not implemented, the strong inherent decoherence of the quantum computer causes the probabilities to quickly decay, as demonstrated by the increasing simulation error in Figure 3b and further discussed in Appendix C. On the other hand, when ZNE is implemented, we observe that the probabilities decay slower as demonstrated in Appendix C. This slow decay is an effect produced by the abrupt truncation of the harmonic oscillator chain, and not by the inherent noise in the quantum computer. The cause for this effect can also be understood by performing a classical simulation without noise of the quantum circuits and comparing its simulation error with the one from the tMPS simulation, as we show in Figure 3c. As illustrated, increasing the number of encoded oscillators in the quantum circuit from l=5to l=7, the error of the quantum circuit simulation is reduced for long simulation times. Further increase of ldoes not result in accuracy improvements. Moreover, the choice of using higher-dimensional harmonic oscillators in the simulation does not appreciably impact the accuracy

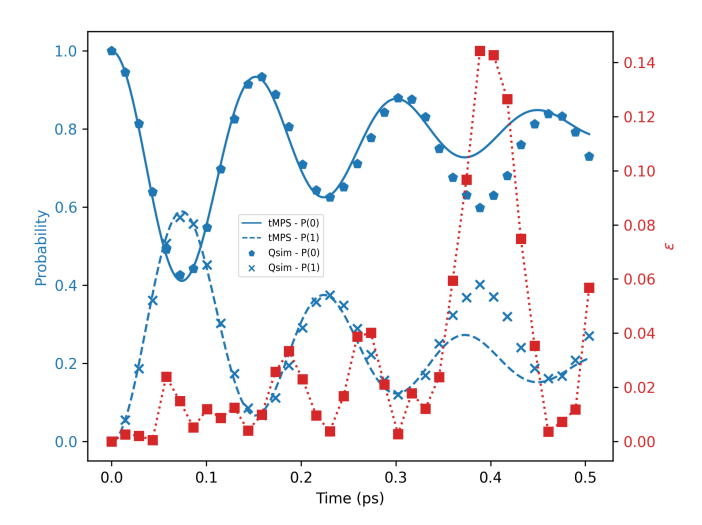


FIG. 4: Results of the simulation of a nonzero temperature environment using Q-TEDOPA. We compare the classical simulation of the quantum circuits (Qsim) with the numerical exact tMPS simulation. The quantum circuit simulation comprises chains of two-dimensional harmonic oscillators of length l=12. In red, we show its error as defined in the text.

of the results as shown by the error of the tMPS simulations (relatively to the numerical exact one) executed with different dimensions d in Figure 3c.

Lastly, we employed Q-TEDOPA to simulate an environment with nonzero temperature. The environment is described by the temperature-dependent spectral density $J_{\beta}(\omega)$ defined in equation (10). We chose a temperature of T = 30K for the environment and an exponentially decaying Ohmic spectral density defined for positive and negative frequencies, as $J(\omega) = 2\pi\alpha\omega e^{-\omega/\omega_c}$, where $\alpha = 0.05$, $\omega_c = 100 cm^{-1}$ and the hard-cutoff frequencies are $\omega_{max} = -\omega_{min} = 10\omega_c$ (more details at Appendix C). We simulated the evolution of the total system through classical simulation of the quantum circuits (without noise), which we compared to a numerical exact tMPS simulation (see Appendix D). The simulations' results and error are shown in Figure 4. The error of the quantum circuit simulation is larger for longer times, a feature that we found to be associated with the abrupt truncation of the harmonic oscillator chains in the quantum circuit.

To conclude, we proposed, implemented and demonstrated with proof-of-concept simulations the versions of the TEDOPA and T-TEDOPA on a quantum computer. As the quantum hardware of NISQ devices improve, we expect the Q-TEDOPA to reach increasingly longer simulation times and to simulate larger systems, making this quantum method an efficient alternative to simulate nonperturbative open quantum system dynamics relatively to the HEOM or the conventional TEDOPA. We envisage that, in the future, it may be of great interest to apply Q-TEDOPA to the work in reference [51], where the photosynthetic exciton transport may be simulated efficiently

beyond dimer systems, i.e. for general light-harvesting complexes. Additional applications are Hamiltonian dynamics simulations of general quantum biological systems [40, 52] and condensed matter systems [53–55] where perturbative approaches fail to provide answers. In the future, it would be interesting to implement optimizations to reduce the harmonic oscillator chain length in the same spirit as the ones reported in reference [56] and to find applications of the Q-TEDOPA to more general quantum computing problems besides quantum simulation.

ACKNOWLEDGMENTS

This work is financed by the ERDF - European Regional Development Fund through the Operational Programme for Competitiveness and Internationalisation - COMPETE 2020 under the Portugal 2020 Partnership Agreement and by National Funds through the FCT - Fundação para a Ciência e a Tecnologia, I.P. (Portuguese Foundation for Science and Technology) within project IBEX, with reference PTDC/CCI-COM/4280/2021. Funding from the Portuguese Foundation for Science and Technology (FCT) in the framework of the Strategic Financing UID/FIS/04650/2020 is acknowledged. José D. Guimarães thanks the FCT for support through PhD grant UI/BD/151173/2021. We acknowledge the utilization of IBM quantum computers through QuantaLab agreement and thank Gonçalo Catarina for helpful discussions.

Appendix A: Bosonic operator mapping

In this section, we show how to map bosonic creation and annihilation operators to Pauli operators using unary and binary qubit encondings for d-dimensional harmonic oscillators. We discuss the complexity of implementing the bosonic hopping term in the chain Hamiltonian (7), since the exponentiation of this term is the one that requires the highest number of CNOT gates in a quantum circuit. The mapping of the remaining Hamiltonian terms follow trivially from the former.

1. Unary qubit encoding

Each harmonic oscillator is represented by an array of d qubits, where the leftmost qubit represents the energy level m=0 and the rightmost qubit represents the m=d energy level. The states $|1\rangle_j$ and $|0\rangle_j$ of the jth qubit represents the case where the harmonic oscillator is in the energy level m=j and $m\neq j$, respectively. In this encoding, the phonon creation operator b^\dagger and phonon

annihilation operator b are given by,

$$b^{\dagger} = \sum_{j=0}^{d-1} \sqrt{j+1} |0\rangle \langle 1|_{j} \otimes |1\rangle \langle 0|_{j+1},$$

$$b = \sum_{j=0}^{d-1} \sqrt{j+1} |1\rangle \langle 0|_{j} \otimes |0\rangle \langle 1|_{j+1}.$$
(A1)

One can map the previous operators to Pauli operators as $|0\rangle\langle 1| = \frac{1}{2}(\hat{X} + i\hat{Y})$ and $|1\rangle\langle 0| = \frac{1}{2}(\hat{X} - i\hat{Y})$.

In reference [30], it has been shown that the unary qubit encoding of an operator with $O(d^2)$ non-zero entries, such as the bosonic hopping term in the Hamiltonian (7), requires, in the worst case, a number of CNOT gates that scales as $O(d^2)$. In practice, optimizations may be performed, e.g. removing equal adjacent gates or parallelizing the application of different Hamiltonian term's evolution operators across different qubits, effectively reducing the quantum circuit depth.

2. Binary qubit encoding

We represent each harmonic oscillator by an array of d qubits, where the leftmost qubit corresponds to the Most Significant Bit (MSB) and the rightmost corresponds to the Least Significant Bit (LSB). Each state comprising the set of log(d) qubits encodes an energy level m of the harmonic oscillator, for instance $|m=3\rangle = |0\rangle \otimes \cdots \otimes |0\rangle \otimes |1\rangle \otimes |1\rangle$. From this, it follows that,

$$b = \sum_{m=1}^{2^{d}-1} \sqrt{m} |m-1\rangle \langle m|,$$

$$b^{\dagger} = \sum_{m=0}^{2^{d}-2} \sqrt{m+1} |m+1\rangle \langle m|.$$
(A2)

The operators $|m+1\rangle\langle m|$ and $|m-1\rangle\langle m|$ must be converted to Pauli operators for each m. One may efficiently obtain the Pauli strings of a term $b_n^\dagger b_{n-1} + b_{n-1}^\dagger b_n$ in binary qubit encoding for an arbitrary d by constructing the sparse matrix of the operator and using a matrix-to-Pauli decomposition technique, such as the one available in the package Pennylane [57]. For d=2, the resulting decomposition is given as $b_n^\dagger b_{n-1} + b_{n-1}^\dagger b_n = \frac{1}{2} \left[\hat{X}_n \hat{X}_{n-1} + \hat{Y}_n \hat{Y}_{n-1} \right]$.

As shown in reference [30], the bosonic hopping term in the Hamiltonian (7) written in binary qubit encoding requires, in the worst case, a number of CNOT gates that scales as $O(d^2 \log(d))$.

Appendix B: Quantum simulation numerical values

1. System Hamiltonian coefficients

The excited state energies ϵ_m and electromagnetic coupling g in the system Hamiltonian (12) were picked from the first two molecules in the FMO complex of green sulphur bacteria (*Cb. tepidum*) results reported in reference [58]. These are $\epsilon_0 = 12410 \ cm^{-1}$, $\epsilon_1 = 12530 \ cm^{-1}$ and $g = 87.7 \ cm^{-1}$.

2. Spectral density

The spectral density in equation (13) was chosen such that a moderate coupling strength between the open quantum system and the non-Markovian environment was present in the simulation. This spectral density allows us to highlight the main feature of TEDOPA and Q-TEDOPA, i.e. that it can simulate the evolution of an open quantum system in the regime where neither Förster or Redfield perturbative theories apply [40]. We chose the hard frequency cutoff value of $\omega_{max} = 10\omega_c$ such that the missing environmental reorganization energy $\lambda_{miss} = \int_{\omega_{max}}^{\infty} d\omega J(\omega)/\omega$ is very small relatively to the total reorganization energy of the environment [29], $\lambda = \int_{0}^{\infty} d\omega J(\omega)/\omega$, i.e. $\lambda_{miss}/\lambda \approx 4.5 \times 10^{-5}$. For the spectral density $J_{\beta}(\omega)$ simulated in this work, one has $\lambda_{miss} = \int_{-\infty}^{\infty} d\omega J(\omega)/\omega$, from where we also obtained $\lambda_{miss}/\lambda \approx 4.5 \times 10^{-5}$. Therefore, the hard cutoff frequencies have a negligible impact on the accuracy of the simulations. We illustrate in Figure 5 the spectral density (13) used in this work.

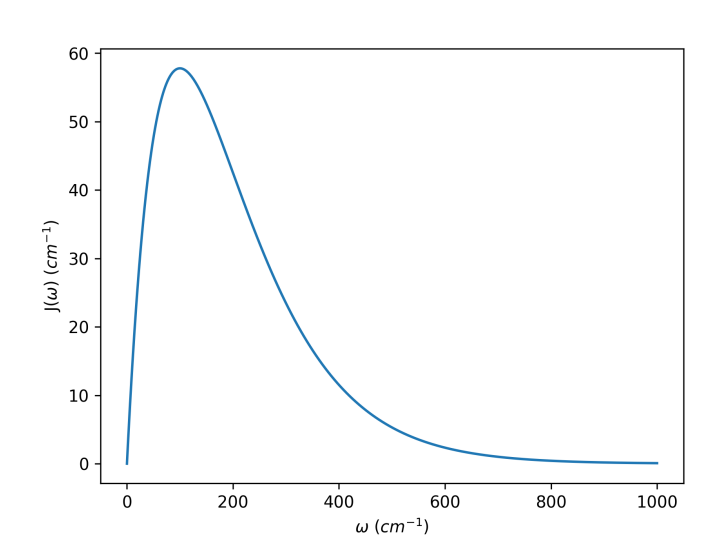


FIG. 5: Exponential decaying Ohmic spectral density as per equation (13).

3. Values of the chain Hamiltonian coefficients

Herein, we report the values of the chain Hamiltonian coefficients for the spectral density at T = 0K defined in equation (13).

The exciton-harmonic oscillator interaction coefficient is $t_0 = 70.69 \ cm^{-1}$.

n	$w_n \ (cm^{-1})$	$t_{n+1,n} \ (cm^{-1})$
0	199.55	139.97
1	385.14	222.93
2	495.81	253.56
3	514.13	253.63
4	507.85	

At the limit $n \to \infty$, one has $t_{n+1,n} = 250 \text{ cm}^{-1}$ and $w_n = 500 \text{ cm}^{-1}$.

Appendix C: Implementation of the quantum simulation

1. Hardcore boson qubit encoding

We restrict the dynamics of the open quantum system to the single-excitation Hilbert subspace where the relevant physics lies; hence excitons behave as hardcore bosons. The exciton creation and annihilation operators c_m^{\dagger} and c_m , respectively, act on a qubit as follows,

$$\begin{aligned} c_m^{\dagger} & |0\rangle_m = |1\rangle_m \,, \\ c_m^{\dagger} & |1\rangle_m = 0, \\ c_m & |0\rangle_m = 0, \\ c_m & |1\rangle_m = |0\rangle_m \,. \end{aligned} \tag{C1}$$

We map the excitonic operators to Pauli operators following a hardcore boson qubit encoding,

$$c_m^{\dagger} = |1\rangle \langle 0| = \frac{1}{2} (\hat{X}_m - i\hat{Y}_m),$$

$$c_m = |0\rangle \langle 1| = \frac{1}{2} (\hat{X}_m + i\hat{Y}_m),$$

$$c_m^{\dagger} c_m = \frac{1}{2} (\hat{I} - \hat{Z}_m).$$
(C2)

2. Trotter-Suzuki product formula implementation

The evolution operator is decomposed using a first-order Trotter-Suzuki product formula,

$$e^{-iHt} \approx \left[e^{-iH_{sing}t/N} e^{-iH_{even}t/N} e^{-iH_{odd}t/N} \right]^N$$
. (C3)

The simulated Hamiltonian is $H = H_S + H^C$ and N is the number of Trotter iterations. We label the qubits in the quantum circuit as even and odd qubits and apply the corresponding two-qubit Hamiltonian terms in H as H_{odd} and H_{even} . The former represents the Hamiltonian terms orderly applied to odd and even labeled qubits and the latter are Hamiltonian terms orderly applied to even and odd labeled qubits. The Hamiltonian terms H_{sing} correspond to single-qubit operations, e.g. $c_m^{\dagger}c_m$. Figure 6 illustrates the implementation of one iteration of the Trotter evolution for a 6 qubit simulation with two-level harmonic oscillators. The generalization for simulations with d-level harmonic oscillators is performed by assigning the even and odd labels in the Hamiltonian terms to even and odd harmonic oscillators (in contrast to qubit assignment as explained above).

3. State initialization, qubit measurement and quantum error mitigation

We initialize all harmonic oscillators in the vacuum state $|0\rangle$ and the molecular qubits in the state $|10\rangle$, i.e. first molecule in the excited state and the second molecule in the ground state. After evolving the system with N Trotter iterations, we measure the probability of obtaining states $|01\rangle$ and $|10\rangle$ in the molecular qubits. We measure only these states in order to mitigate qubit amplitude damping errors. Excitons are conserved in the system, thus this error mitigation technique can be applied. One may admit excitation-preserving dynamics in the photosynthetic exciton transport if the dynamics we want to observe occurs on a timescale much smaller than exciton recombination processes. The transient coherent exciton transport dynamics, i.e. the physics that has the most interest to us (where quantum effects may play a fundamental role), occurs in a timescale less than 1 ps [59, 60], which is about $\sim 10^2 - 10^3$ times smaller than exciton recombination processes [40, 61].

We applied measurement error mitigation in *Qiskit*, a technique that suppresses qubit readout errors. Two other effective error mitigation techniques were implemented in this work namely, the Randomized Compiling (RC) [45, 46] and the Zero-Noise Extrapolation (ZNE)

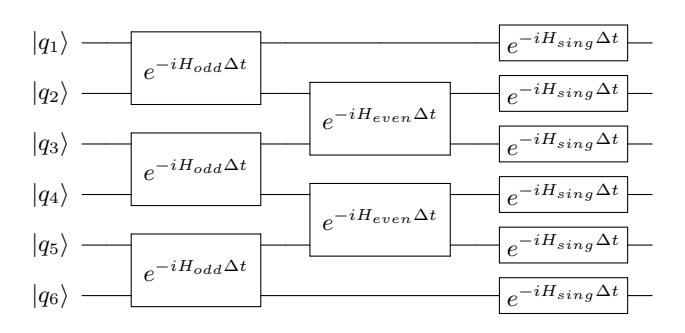


FIG. 6: Implementation of a Trotter iteration in a quantum circuit. The labelled qubits q_1 , q_2 , q_5 and q_6 are harmonic oscillators and the qubits q_3 and q_4 are the molecular qubits. The Trotter time step is $\Delta t = t/N$.

[47, 48]. The former suppresses coherent noise arising from under- and over- rotations of quantum gates by tailoring these errors into stochastic noise. Doing this, we are quadratically reducing the worst-case probability of obtaining an incorrect quantum gate implementation as a function of the average gate infidelity [45]. We applied RC to CNOT gates. The ZNE was also applied by folding the CNOT gates for 1 (no folding) and 3 times (via the Fixed Identity Insertion Method [62]). For each CNOT folding factor, we implemented RC by averaging the results of the 30 randomized compiled quantum circuits, yielding a total of 2×30 executed quantum circuits for each simulation time t. Each circuit was measured 1.6×10^4 times. ZNE allows the user to increase the average error rate in the quantum circuit and then extrapolate to the zero-noise result, hence mitigating errors introduced from different decoherence sources in the quantum computer. We implemented exponential extrapolation [48] using the software Mitiq [49]. The impact of exponential ZNE in the quantum simulation results presented in Figure 3 for the 12 simulated Trotter iterations is explicitly demonstrated in Figure 7. We observe that exponential extrapolation is able to effectively suppress phase damping errors. However, it is unstable, whereas Richardson extrapolation is not very effective but stable for our particular quantum circuits [48]. As discussed in reference [47] and shown recently in reference [63], the joint implementation of RC and ZNE increases the effectiveness of these quantum error mitigation techniques with respect to their individual application.

4. Noise in *ibmq toronto*

In *Qiskit*, one has access to the devices' qubit relaxation times and the duration the quantum circuit takes to be executed. We observed that the quantum digital

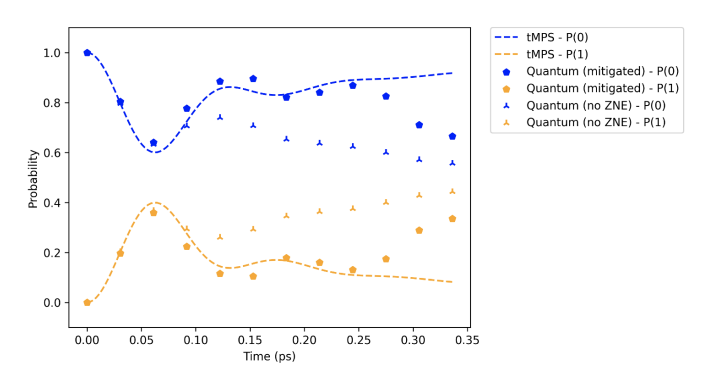


FIG. 7: Results obtained with the quantum simulation in the *ibmq toronto* with (without) the ZNE implemented, as represented by the pentagons (triangles). Numerical exact results obtained with tMPS (dashed lines) are also shown. The results obtained without ZNE contain all other error mitigation techniques referred in the text applied in the simulation.

simulation of 12 Trotter iterations with optimization level 1, pulses' scheduling method "as late as possible", and a system cycle time (ibmq toronto) of dt=0.22~ns takes $\approx 47~\mu s$ to be executed. The average $T_1~(T_2)$ relaxation time when we executed the quantum circuits was $\approx 82~\mu s~(\approx 103~\mu s)$, therefore we expect non-negligible effects from qubit phase damping and, in particular, amplitude damping in the simulation results, as shown in Figure 7. We remark that the limit of infinite noise is obtained when P(0)=P(1)=0.5 because we are measuring the molecular qubit states $|01\rangle$ and $|10\rangle$, both approximately equally affected by the amplitude damping noise.

The decay of the last 3 Trotter iterations in the results shown in Figure 7 (with ZNE implemented) is due to the truncated harmonic oscillator chain length. The abrupt truncation of the chain at l = 5 induces a full reflection of the bosonic excitations that travel forward in the chain. Allowing enough time for the simulation, these artificial reflected excitations travel back through the chain again and interact with the system, producing unrealistic dynamics of the open system. This is demonstrated by the results in Figure 8 obtained by classical simulations of the quantum circuits without noise. Given a simulation time length t, two simulations with different chain lengths, i.e. l=5 and l'=7, we observe that the open quantum system dynamics with the latter chain follow the numerical exact results up to the 12th Trotter iteration, whereas in the former the effects of the reflection of the bosonic excitations at the edge of the truncated chain are clearly visible. Note that the unrealistic probability decay obtained in the results with l=5 is similar to the decay we observed in the quantum simulation results (with ZNE implemented) in Figure 7, hence we conclude that the abrupt truncation of the chain introduces the artificial

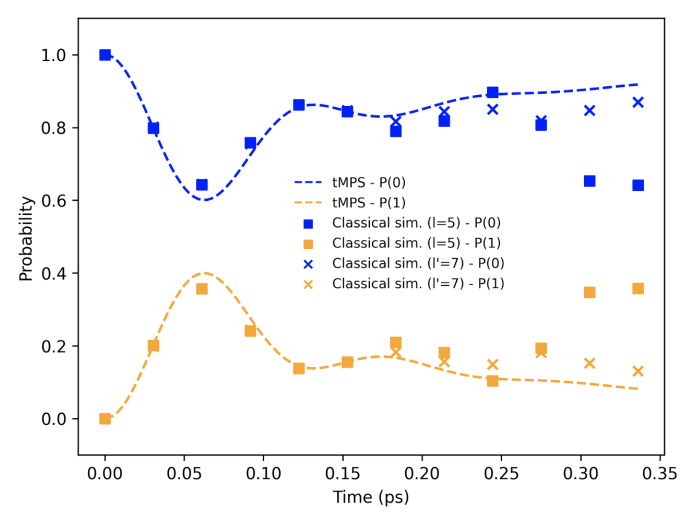


FIG. 8: Results obtained by the classical simulations of the quantum circuits (without noise). Results for a simulated chain length of l=5 (l'=7) are given by squares (crosses) and the numerical exact tMPS results are given by dashed lines.

behaviour of the dynamics.

Appendix D: Matrix Product State simulation

The classically computed numerical exact results were obtained using the tMPS technique [8]. We decomposed the evolution operator using a second-order Trotter-Suzuki product formula and applied SVD compression

- to each resulting Matrix Product Operator, allowing for a truncation error $\epsilon > 0$, upper bounded by $\epsilon < 10^{-4}$. The Matrix Product States were compressed after each Trotter iteration with SVD, where we allowed a truncation error upper bounded by $\epsilon < 10^{-8}$. The TEDOPA (T-TEDOPA) simulation of the environment at T = 0K (T = 30K) consisted of chains of harmonic oscillators with dimension d = 8 (d = 8), chains' length l = 15 (l = 35) and 120 (180) Trotter iterations.
- Y. Tanimura, Numerically "exact" approach to open quantum dynamics: The hierarchical equations of motion (heom), The Journal of chemical physics 153, 020901 (2020).
- [2] A. Ishizaki and G. R. Fleming, Unified treatment of quantum coherent and incoherent hopping dynamics in electronic energy transfer: Reduced hierarchy equation approach, The Journal of chemical physics 130, 234111 (2009).
- [3] K. Nakamura and Y. Tanimura, Optical response of laser-driven charge-transfer complex described by holstein-hubbard model coupled to heat baths: Hierarchical equations of motion approach, The Journal of Chemical Physics 155, 064106 (2021).
- [4] A. W. Chin, S. F. Huelga, and M. B. Plenio, Chain representations of open quantum systems and their numerical simulation with time-adaptive density matrix renormalisation group methods, in *Semiconductors and Semimetals*, Vol. 85 (Elsevier, 2011) pp. 115–143.
- [5] A. W. Chin, Á. Rivas, S. F. Huelga, and M. B. Plenio, Exact mapping between system-reservoir quantum models and semi-infinite discrete chains using orthogonal polynomials, Journal of Mathematical Physics 51, 092109 (2010).
- [6] J. Prior, A. W. Chin, S. F. Huelga, and M. B. Plenio, Efficient simulation of strong system-environment interactions, Physical review letters 105, 050404 (2010).
- [7] D. Tamascelli, A. Smirne, J. Lim, S. F. Huelga, and M. B. Plenio, Efficient simulation of finite-temperature open quantum systems, Physical review letters 123, 090402 (2019).
- [8] U. Schollwöck, The density-matrix renormalization group in the age of matrix product states, Annals of physics **326**, 96 (2011).
- [9] J. Eisert, M. Cramer, and M. B. Plenio, Colloquium: Area laws for the entanglement entropy, Reviews of modern physics 82, 277 (2010).
- [10] G. A. Quantum, Collaborators*†, F. Arute, K. Arya, R. Babbush, D. Bacon, J. C. Bardin, R. Barends, S. Boixo, M. Broughton, B. B. Buckley, et al., Hartreefock on a superconducting qubit quantum computer, Science 369, 1084 (2020).
- [11] F. Arute, K. Arya, R. Babbush, D. Bacon, J. C. Bardin, R. Barends, A. Bengtsson, S. Boixo, M. Broughton, B. B. Buckley, et al., Observation of separated dynamics of charge and spin in the fermi-hubbard model, arXiv preprint arXiv:2010.07965 (2020).
- [12] F. Arute, K. Arya, R. Babbush, D. Bacon, J. C. Bardin, R. Barends, R. Biswas, S. Boixo, F. G. Brandao, D. A.

- Buell, et al., Quantum supremacy using a programmable superconducting processor, Nature **574**, 505 (2019).
- [13] Y. Wu, W.-S. Bao, S. Cao, F. Chen, M.-C. Chen, X. Chen, T.-H. Chung, H. Deng, Y. Du, D. Fan, et al., Strong quantum computational advantage using a superconducting quantum processor, Physical review letters 127, 180501 (2021).
- [14] C. Ye, C. M. Hill, S. Wu, J. Ruan, and Z. S. Ma, Dbg2olc: efficient assembly of large genomes using long erroneous reads of the third generation sequencing technologies, Scientific reports 6, 1 (2016).
- [15] A. W. Schlimgen, K. Head-Marsden, L. M. Sager, P. Narang, and D. A. Mazziotti, Quantum simulation of open quantum systems using a unitary decomposition of operators, Physical Review Letters 127, 270503 (2021).
- [16] B. Rost, L. Del Re, N. Earnest, A. F. Kemper, B. Jones, and J. K. Freericks, Demonstrating robust simulation of driven-dissipative problems on near-term quantum computers, arXiv preprint arXiv:2108.01183 (2021).
- [17] S. Tornow, W. Gehrke, and U. Helmbrecht, Nonequilibrium dynamics of a dissipative two-site hubbard model simulated on ibm quantum computers, arXiv preprint arXiv:2011.11059 (2020).
- [18] G. García-Pérez, M. A. Rossi, and S. Maniscalco, Ibm q experience as a versatile experimental testbed for simulating open quantum systems, npj Quantum Information 6. 1 (2020).
- [19] S. Endo, J. Sun, Y. Li, S. C. Benjamin, and X. Yuan, Variational quantum simulation of general processes, Physical Review Letters 125, 010501 (2020).
- [20] X. Yuan, S. Endo, Q. Zhao, Y. Li, and S. C. Benjamin, Theory of variational quantum simulation, Quantum 3, 191 (2019).
- [21] B. Rost, B. Jones, M. Vyushkova, A. Ali, C. Cullip, A. Vyushkov, and J. Nabrzyski, Simulation of thermal relaxation in spin chemistry systems on a quantum computer using inherent qubit decoherence, arXiv preprint arXiv:2001.00794 (2020).
- [22] S. Sun, L.-C. Shih, and Y.-C. Cheng, Efficient quantum simulation of open quantum system dynamics on noisy quantum computers, arXiv preprint arXiv:2106.12882 (2021).
- [23] A. Di Paolo, P. K. Barkoutsos, I. Tavernelli, and A. Blais, Variational quantum simulation of ultrastrong lightmatter coupling, Physical Review Research 2, 033364 (2020).
- [24] A. Macridin, P. Spentzouris, J. Amundson, and R. Harnik, Digital quantum computation of fermionboson interacting systems, Physical Review A 98, 042312 (2018).

- [25] H. Kamakari, S.-N. Sun, M. Motta, and A. J. Minnich, Digital quantum simulation of open quantum systems using quantum imaginary—time evolution, PRX Quantum 3, 010320 (2022).
- [26] J. D. Guimarães, C. Tavares, L. S. Barbosa, and M. I. Vasilevskiy, Simulation of nonradiative energy transfer in photosynthetic systems using a quantum computer, Complexity 2020 (2020).
- [27] W. Gautschi, Algorithm 726: Orthpol-a package of routines for generating orthogonal polynomials and gausstype quadrature rules, ACM Transactions on Mathematical Software (TOMS) 20, 21 (1994).
- [28] M. Woods, R. Groux, A. Chin, S. F. Huelga, and M. B. Plenio, Mappings of open quantum systems onto chain representations and markovian embeddings, Journal of Mathematical Physics 55, 032101 (2014).
- [29] D. Tamascelli, Excitation dynamics in chain-mapped environments, Entropy 22, 1320 (2020).
- [30] N. P. Sawaya, T. Menke, T. H. Kyaw, S. Johri, A. Aspuru-Guzik, and G. G. Guerreschi, Resourceefficient digital quantum simulation of d-level systems for photonic, vibrational, and spin-s hamiltonians, npj Quantum Information 6, 1 (2020).
- [31] B. D. Jones, D. R. White, G. O. O'Brien, J. A. Clark, and E. T. Campbell, Optimising trotter-suzuki decompositions for quantum simulation using evolutionary strategies, in *Proceedings of the Genetic and Evolutionary* Computation Conference (2019) pp. 1223–1231.
- [32] B. Şahinoğlu and R. D. Somma, Hamiltonian simulation in the low-energy subspace, npj Quantum Information 7, 1 (2021).
- [33] D. W. Berry, A. M. Childs, R. Cleve, R. Kothari, and R. D. Somma, Simulating hamiltonian dynamics with a truncated taylor series, Physical review letters 114, 090502 (2015).
- [34] G. H. Low and I. L. Chuang, Hamiltonian simulation by qubitization, Quantum 3, 163 (2019).
- [35] Y. Li and S. C. Benjamin, Efficient variational quantum simulator incorporating active error minimization, Physical Review X 7, 021050 (2017).
- [36] C. Cirstoiu, Z. Holmes, J. Iosue, L. Cincio, P. J. Coles, and A. Sornborger, Variational fast forwarding for quantum simulation beyond the coherence time, npj Quantum Information 6, 1 (2020).
- [37] B. Commeau, M. Cerezo, Z. Holmes, L. Cincio, P. J. Coles, and A. Sornborger, Variational hamiltonian diagonalization for dynamical quantum simulation, arXiv preprint arXiv:2009.02559 (2020).
- [38] S. Barison, F. Vicentini, and G. Carleo, An efficient quantum algorithm for the time evolution of parameterized circuits, Quantum 5, 512 (2021).
- [39] N. F. Berthusen, T. V. Trevisan, T. Iadecola, and P. P. Orth, Quantum dynamics simulations beyond the coherence time on nisq hardware by variational trotter compression, arXiv preprint arXiv:2112.12654 (2021).
- [40] M. Mohseni, Y. Omar, G. S. Engel, and M. B. Plenio, Quantum effects in biology (Cambridge University Press, 2014).
- [41] J. Jeske, D. J. Ing, M. B. Plenio, S. F. Huelga, and J. H. Cole, Bloch-redfield equations for modeling lightharvesting complexes, The Journal of chemical physics 142, 064104 (2015).
- [42] Z. Li, L. Ko, Z. Yang, M. Sarovar, and K. B. Whaley, Interplay of vibration-and environment-assisted energy

- transfer, New Journal of Physics.
- [43] G. McCauley, B. Cruikshank, D. I. Bondar, and K. Jacobs, Accurate lindblad-form master equation for weakly damped quantum systems across all regimes, npj Quantum Information 6, 1 (2020).
- [44] A. Cross, The ibm q experience and qiskit open-source quantum computing software, in APS March meeting abstracts, Vol. 2018 (2018) pp. L58–003.
- [45] A. Hashim, R. K. Naik, A. Morvan, J.-L. Ville, B. Mitchell, J. M. Kreikebaum, M. Davis, E. Smith, C. Iancu, K. P. O'Brien, et al., Randomized compiling for scalable quantum computing on a noisy superconducting quantum processor, arXiv preprint arXiv:2010.00215 (2020).
- [46] J. J. Wallman and J. Emerson, Noise tailoring for scalable quantum computation via randomized compiling, Physical Review A 94, 052325 (2016).
- [47] Y. Li and S. C. Benjamin, Efficient variational quantum simulator incorporating active error minimization, Physical Review X 7, 021050 (2017).
- [48] T. Giurgica-Tiron, Y. Hindy, R. LaRose, A. Mari, and W. J. Zeng, Digital zero noise extrapolation for quantum error mitigation, in 2020 IEEE International Conference on Quantum Computing and Engineering (QCE) (IEEE, 2020) pp. 306–316.
- [49] R. LaRose, A. Mari, S. Kaiser, P. J. Karalekas, A. A. Alves, P. Czarnik, M. E. Mandouh, M. H. Gordon, Y. Hindy, A. Robertson, et al., Mitiq: A software package for error mitigation on noisy quantum computers, arXiv preprint arXiv:2009.04417 (2020).
- [50] S. Endo, Z. Cai, S. C. Benjamin, and X. Yuan, Hybrid quantum-classical algorithms and quantum error mitigation, Journal of the Physical Society of Japan 90, 032001 (2021).
- [51] A. Chin, J. Prior, R. Rosenbach, F. Caycedo-Soler, S. F. Huelga, and M. B. Plenio, The role of non-equilibrium vibrational structures in electronic coherence and recoherence in pigment-protein complexes, Nature Physics 9, 113 (2013).
- [52] N. Christensson, H. F. Kauffmann, T. Pullerits, and T. Mancal, Origin of long-lived coherences in lightharvesting complexes, The Journal of Physical Chemistry B 116, 7449 (2012).
- [53] M. Vasilevskiy, E. Anda, and S. Makler, Electronphonon interaction effects in semiconductor quantum dots: A nonperturabative approach, Physical Review B 70, 035318 (2004).
- [54] M. Wang, M. Hertzog, and K. Börjesson, Polaritonassisted excitation energy channeling in organic heterojunctions, Nature communications 12, 1 (2021).
- [55] S. Rafiq, B. Fu, B. Kudisch, and G. D. Scholes, Interplay of vibrational wavepackets during an ultrafast electron transfer reaction, Nature chemistry 13, 70 (2021).
- [56] M. Sánchez-Barquilla and J. Feist, Accurate truncations of chain mapping models for open quantum systems, Nanomaterials 11, 2104 (2021).
- [57] e. a. Bergholm, Ville, Pennylane: Automatic differentiation of hybrid quantum-classical computations., arXiv preprint arXiv:1811.04968 (2018).
- [58] J. Adolphs and T. Renger, How proteins trigger excitation energy transfer in the fmo complex of green sulfur bacteria, Biophysical journal 91, 2778 (2006).
- [59] G. S. Engel, T. R. Calhoun, E. L. Read, T.-K. Ahn, T. Mančal, Y.-C. Cheng, R. E. Blankenship, and G. R.

- Fleming, Evidence for wavelike energy transfer through quantum coherence in photosynthetic systems, Nature **446**, 782 (2007).
- [60] G. Panitchayangkoon, D. Hayes, K. A. Fransted, J. R. Caram, E. Harel, J. Wen, R. E. Blankenship, and G. S. Engel, Long-lived quantum coherence in photosynthetic complexes at physiological temperature, Proceedings of the National Academy of Sciences 107, 12766 (2010).
- [61] J. Dostál, J. Pšenčík, and D. Zigmantas, In situ mapping of the energy flow through the entire photosynthetic apparatus, Nature Chemistry 8, 705 (2016).
- [62] C. Bauer, A. He, W. A. de Jong, B. Nachman, and V. R. Pascuzzi, Computationally efficient zero noise extrapolation for quantum gate error mitigation, arXiv preprint arXiv:2110.13338 (2021).
- [63] N. F. Berthusen, T. V. Trevisan, T. Iadecola, and P. P. Orth, Quantum dynamics simulations beyond the coherence time on nisq hardware by variational trotter compression, arXiv preprint arXiv:2112.12654 (2021).
- [64] J. D. Guimarães, C. Tavares, L. S. Barbosa, and M. I. Vasilevskiy, Simulation of nonradiative energy transfer in photosynthetic systems using a quantum computer, Complexity 2020 (2020).
- [65] S.-H. Yeh, R. D. Hoehn, M. A. Allodi, G. S. Engel, and S. Kais, Elucidation of near-resonance vibronic coherence lifetimes by nonadiabatic electronic-vibrational state character mixing, Proceedings of the National Academy of Sciences 116, 18263 (2019).
- [66] M. A. Nielsen and I. Chuang, Quantum computation and quantum information (2002).
- [67] Z. Cai, Multi-exponential error extrapolation and combining error mitigation techniques for nisq applications, npj Quantum Information 7, 1 (2021).